BIOCHEMISTRY
including biophysical chemistry & molecular biology

Article

pubs.acs.org/biochemistry

Cholesterol-Dependent Conformational Exchange of the C-Terminal Domain of the Influenza A M2 Protein

Sangwoo S. Kim,[†] Mary Alice Upshur,[†] Kei Saotome,[†] Indra D. Sahu,[‡] Robert M. McCarrick,[‡] Jimmy B. Feix,[§] Gary A. Lorigan,[‡] and Kathleen P. Howard*[,†]

[†]Department of Chemistry and Biochemistry, Swarthmore College, Swarthmore, Pennsylvania 19081, United States

[‡]Department of Chemistry and Biochemistry, Miami University, Oxford, Ohio 45056, United States

[§]Department of Biophysics, National Biomedical EPR Center, Medical College of Wisconsin, Milwaukee, Wisconsin 53226, United States

Supporting Information

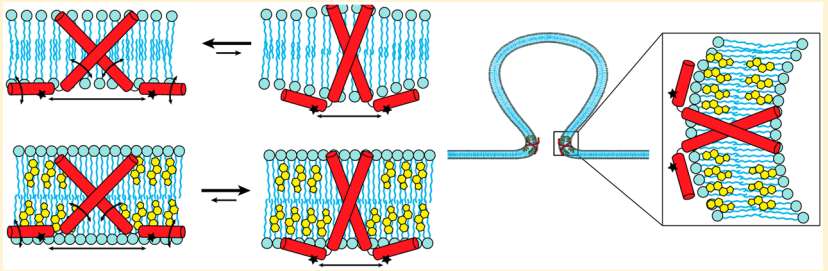

ABSTRACT: The C-terminal amphipathic helix of the influenza A M2 protein plays a critical cholesterol-dependent role in viral budding. To provide atomic-level detail on the impact cholesterol has on the conformation of M2 protein, we spin-labeled sites right before and within the C-terminal amphipathic helix of the M2 protein. We studied the spin-labeled M2 proteins in membranes both with and without cholesterol. We used a multipronged site-directed spin-label electron paramagnetic resonance (SDSL-EPR) approach and collected data on line shapes, relaxation rates, accessibility of sites to the membrane, and distances between symmetry-related sites within the tetrameric protein. We demonstrate that the C-terminal amphipathic helix of M2 populates at least two conformations in POPC/POPG 4:1 bilayers. Furthermore, we show that the conformational state that becomes more populated in the presence of cholesterol is less dynamic, less membrane buried, and more tightly packed than the other state. Cholesterol-dependent changes in M2 could be attributed to the changes cholesterol induces in bilayer properties and/or direct binding of cholesterol to the protein. We propose a model consistent with all of our experimental data that suggests that the predominant conformation we observe in the presence of cholesterol is relevant for the understanding of viral budding.

Influenza A viruses cause recurrent seasonal epidemics and global pandemics.[1,2] The threat of future pandemics coupled with growing resistance to current antivirals makes the development of new antiviral influenza drugs a national healthcare priority.[3] A series of recently published papers provides new insight into how influenza virus buds at the plasma membrane of infected cells.[4−6] An atomic-level understanding of the budding process could lead to strategies to inhibit the replication of viruses and new tactics for inhibiting viral infectivity.[7] One of the proteins found on the viral coat of influenza, the M2 protein, has been shown to be critical to viral budding[5,6,8] and is the focus of this article.

The M2 protein is a multifunctional membrane-bound protein that acts at several stages of the virus lifecycle.[9] Each 97 amino acid monomer within the homotetrameric protein consists of a N-terminal ectodomain, a transmembrane domain, and a C-terminal cytoplasmic domain.[9] The most extensively studied function of the M2 protein is its proton channel activity, mediated by the transmembrane domain, that is crucial for the uncoating of virions when viruses enter cells. More recently, the C-terminal domain of M2 has been shown to play a critical role in viral budding, which is an essential step in the replication cycle of influenza.[8,10]

Deletion mutants provided initial evidence that the C-terminal region of the M2 protein is critical for infectivity and virus morphology.[11] Further deletion studies and alanine-scanning experiments by several groups identified residues ∼46−61 as being critical to viral budding.[5,6,12] An *in vitro* assay has been used to probe the 46−61 region and demonstrated that both the full-length protein as well as just the 46−61 region are capable of inducing budding in giant unilamellar vesicles.[8]

Several groups, including our own, have demonstrated that the 46−60 residue region forms an amphipathic membrane-surface helix.[13,14] Amphipathic membrane-surface helices have been shown to promote curvature in several systems,[15−17]

Received: September 29, 2015
Revised: November 15, 2015
Published: November 16, 2015

DOI: 10.1021/acs.biochem.5b01065
Biochemistry 2015, 54, 7157−7167

presumably due to their ability to cause lipid-packing defects that induce curvature. As a homotetramer, the M2 protein contains four amphipathic helices, but it is not understood how the four helices are arranged with respect to each other and how they work in concert to promote viral budding.

Site-directed spin-label EPR spectroscopy (SDSL-EPR) has proven to be a powerful method for studying membrane proteins reconstituted into lipid bilayers[18] and can provide conformational insight not accessible from other biophysical techniques. Structural parameters measured in SDSL-EPR experiments include distances from ~12−60 Å, the topology of a membrane protein with respect to a lipid bilayer, and mobility information on multiple time scales.[19] Our group has previously published several SDSL-EPR studies on M2.[13,20−23] As part of this work, we demonstrated that the conformation and dynamics of the C-terminal amphipathic helix of M2 changes in response to pH[13] and the addition of adamantine drugs.[20]

Influenza budding studies have shown that viral budding is cholesterol-dependent.[4] It has been hypothesized that cholesterol is necessary for guiding M2 to the edge of an infected cell's cholesterol-rich budozone and for M2's ability to promote curvature for viral budding.[24] Despite extensive study and speculation, atomic-level details of the roles cholesterol might play in viral budding are not understood.[24,25] In this article, we extend our previous SDSL-EPR work on the C-terminal amphipathic helix of M2 and present data on the impact cholesterol has on the conformation and dynamics of this region with the goal of providing insight into the cholesterol dependence of M2's role in viral budding.

For this article, we studied spin-labeled sites right before and within the C-terminal amphipathic helix. Utilizing a multipronged SDSL-EPR approach, we demonstrate that the C-terminal amphipathic helix can exist in at least two conformational states that differ in the depth of the helices in the membrane and how the four helices within the homotetrameric protein are arranged with respect to each other. The populations of these two conformational states shift upon addition of cholesterol to the membrane lipid bilayer.

MATERIALS AND METHODS

Synthesis, Spin Labeling, and Membrane Reconstitution of M2 Peptides. Peptide synthesis and purification were performed as described previously,[13] and the sequences of M2TMC 23−60 peptides are provided in Figure 1B. This 38 residue peptide construct has been used in a large number of structural studies on M2[13,20,26,27] and has been shown to generate the membrane curvature necessary for viral budding.[28] Furthermore, the C-terminal helix in the M2TMC 23−60 peptide has been shown to have the same conformation as the same region in the full-length M2 protein.[21] Peptides were nitroxide spin-labeled using cysteine-specific 1-oxyl-2,2,5,5-tetramethyl-3-pyrroline-3-methylmethanethiosulfonate (MTSL) spin labels.[13]

For line shape analysis and accessibility studies, M2 peptides were reconstituted into lipid bilayers consisting of 1-palmitoyl-2-oleyl-*sn*-glycero-phosphocholine (POPC) and 1-palmitoyl-2-oleyl-*sn*-glycero-3-[phospho-*rac*-(1-glycerol)] (POPG) in a POPC/POPG 4:1 molar ratio. The peptide/lipid molar ratio was 1:200. The reconstitution protocol was described in detail previously.[13] We chose POPC/POPG 4:1 bilayers because an *in vitro* budding assay has demonstrated that the M2 protein can induce curvature and initiate budding in vesicles made of POPC/POPG 4:1.[8] Furthermore, a number of previously published biophysical studies on M2 have utilized POPC/POPG 4:1 bilayers and provide valuable context for this study.[13,20−23] The sample buffer was 50 mM Tris, pH 7.8, 100 mM KCl, 1 mM EDTA.

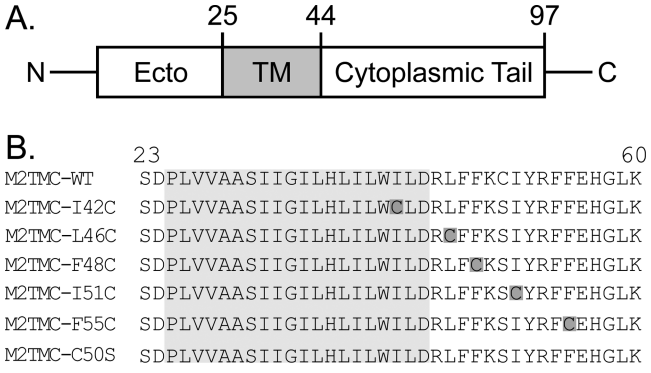

Figure 1. Spin-labeled M2 peptides used in this study. (A) Each monomer of the M2 protein is composed of a N-terminal ectodomain, a transmembrane domain (shaded in gray), and a C-terminal cytoplasmic domain. (B) Wild-type sequence corresponds to the M2 protein from influenza strain A/Udorn/72 (H3N2). M2TMC (23−60) peptides were spin-labeled at single cysteine sites (dark gray boxes). All M2TMC sequences other than the WT sequence have a C50S replacement in addition to the cysteine substitution necessary for spin labeling. The last cysteine-less sequence was used for spin dilution.

For double electron−electron resonance (DEER) EPR samples, M2 peptides were reconstituted into lipid bilayers of POPC/POPG 4:1 at a peptide/lipid 1:300 molar ratio, micelles consisting of 1,2-dihexanoyl-*sn*-glycero-3-phosphocholine (DHPC) at a peptide/detergent 1:500 molar ratio, or bicelles consisting of POPC/POPG/DHPC at a peptide/lipid 1:500 molar ratio. M2 peptides were also reconstituted into Lipodisq nanoparticles composed of POPC/POPG lipid bilayers as previously described.[29] The DEER sample buffer was 50 mM Tris, pH 7.8, 100 mM KCl, 1 mM EDTA in 30% (v/v) glycerol.

For saturation-recovery EPR (SR-EPR) samples, M2 peptides were reconstituted into POPC/POPG 4:1 lipid bilayers at a peptide/lipid 1:500 molar ratio. The samples were spin-diluted by adding unlabeled M2TMC C50S at an unlabeled/labeled 4:1 molar ratio.

EPR Spectroscopy and Data Analysis. Continuous wave (CW) EPR spectra were recorded at room temperature on an X-band Bruker EMX spectrometer equipped with an ER4123D resonator. Samples used for analysis of spectral line shapes were placed in glass capillary tubes, and EPR spectra were acquired using 2 mW incident microwave power, 1 G field modulation amplitude at 100 kHz, and 150 G sweep width. For comparison of line shapes, each spectrum was double integrated and normalized to the same number of spins.

EPR lineshapes were simulated using Multicomponent, a LabView program written by Christian Altenbach. The program fits slow-motion EPR data using a microscopic order macroscopic disorder (MOMD) model.[30] The data were well fit using two components with distinct rotational properties. Initial values for magnetic tensors were taken from previously published data of MTSL dynamics on a solvent-exposed membrane protein α-helix site.[31]

For power saturation measurements, samples were collected in gas-permeable TPX capillary tubes. Power saturation data were obtained under three sets of conditions: equilibrated with

DOI: 10.1021/acs.biochem.5b01065
Biochemistry 2015, 54, 7157−7167

nitrogen gas, equilibrated with ambient air, and equilibrated with nitrogen in the presence of 20 mM nickel(II) ethylenediaminediacetate (NiEDDA). For experiments with low accessibility to fast relaxing paramagnetic reagents, EPR spectra were measured at eight power levels. For experiments with high accessibility to paramagnetic reagents, 16 power levels were studied as the saturation effect was sometimes significantly mitigated and thus more data points were required to achieve a good fit. Data were analyzed and $\Delta P_{1/2}$ parameters reflecting side chain accessibility to paramagnetic reagents were determined as described previously.[13]

Saturation-recovery EPR experiments (SR-EPR) were carried out at the National Biomedical EPR Center on a home-built instrument operating at X-band (9.4 GHz) equipped with a loop-gap resonator.[32] Briefly, samples (5 μL) contained in a gas-permeable TPX capillary were placed under a continuous flow of N_2 mixed with air to give the desired final oxygen concentration. A 1 μs saturating microwave pulse was applied at the absorption maximum of the central ($M_I = 0$) line, followed by signal acquisition with sampling intervals ranging from 2 to 20 ns per point for 2048 points and an overall repetition rate of 40−100 kHz. Total accumulation times varied from 5 to 60 min. The resulting SR signals were fitted with single- and double-exponential decay functions using Origin software (OriginLab, Northampton, MA). Bimolecular collision rates with oxygen, $W_x(O_2)$, were calculated from spin−lattice relaxation rates (W_e) according to the relationship[19,33] $W_x(O_2) = W_e(O_2) - W_e(N_2)$, where $W_e = 1/2T_1$.

Double electron−electron resonance (DEER) EPR experiments were carried out at the Ohio Advanced EPR Laboratory at Miami University, Ohio, on a Bruker ELEXSYS E580 spectrometer equipped with a SuperQ-FT pulse Q-band system with a 10 W amplifier and EN5107D2 resonator.[29] DEER data were collected using the standard four-pulse sequence[34] $[(\pi/2)_{\nu 1} - \tau_1 - (\pi)_{\nu 1} - t - (\pi)_{\nu 2} - (\tau_1 + \tau_2 - t) - (\pi)_{\nu 1} - \tau_2 -$ echo] at Q-band with a probe pulse width of 10/20 ns, pump pulse width of 24 ns, 80 MHz of frequency difference between probe and pump pulse, shot repetition time determined by spin−lattice relaxation rate (T_1), 100 echoes/point, and two-step phase cycling at 80 K for overnight data acquisition time (12 h). The DEER data were analyzed using DEER Analysis 2015,[35] and the distance distributions were extracted by Tikhonov regularization.[36] The regularization parameter was optimized by L-curve calculation using a modified algorithm provided by Dr. Clark Hyde at the University of Chicago.[37]

RESULTS

M2 Conformation and Dynamics Is Sensitive to the Choice of Membrane Mimic. Structural studies of the influenza A M2 protein have been published using membrane mimics ranging from detergent micelles to complex bilayers.[26,38−40] In an effort to reconcile the differences seen in published structures, we collected EPR spectra of M2 in a range of different membrane mimics.

EPR experiments are well-suited to study the impact of membrane environment since the time scale of the spectroscopic measurement allows a wide range of membrane mimics to be employed. In Figure 2, we show EPR spectra of a spin-labeled M2 peptide in a range of different environments used in previously published work. DHPC micelles were used for solution nuclear magnetic resonance spectroscopy (NMR) studies,[26] POPC/POPG bilayers were employed for site-directed spin-label EPR (SDSL-EPR) experiments,[13,20−23] and

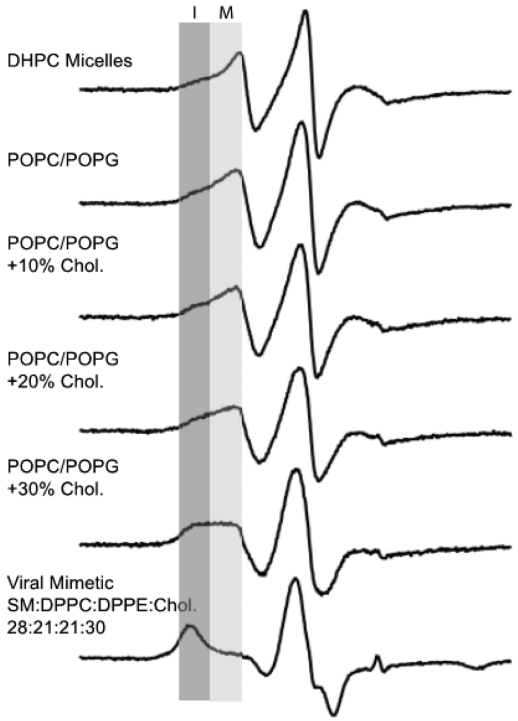

Figure 2. EPR line shape depends on choice of membrane mimic. Normalized X-band CW EPR spectra of M2TMC (23−60) spin labeled at I42C in DHPC micelles, POPC/POPG (4:1) bilayers with varying molar quantities of cholesterol, and a viral membrane mimic (SM/DPPC/DPPE/Chol/PEG−PE 23:21:21:30:1). Each sample was spin-diluted with unlabeled peptide (unlabeled/labeled 4:1) to eliminate broadening resulting from spin-coupling between monomers within the homotetrameric protein. The darker gray box indicates a broader, more immobilized component (I) that increases in intensity from top to bottom. The more mobile component (M) indicated by a lighter gray box decreases in intensity from top to bottom.

viral mimetic membranes (SM/DPPC/DPPE/Chol/PEG−PE 23:21:21:30:1) were used in solid-state NMR (ssNMR) experiments.[41] POPC/POPG bilayers were also used in an *in vitro* budding assay, which demonstrated that adding cholesterol to POPC/POPG bilayers modulates the ability of the M2 protein to initiate budding.[8]

A striking observation from the stack plot of spectra in Figure 2 is that the CW EPR spectra appear to be a superposition of two different spectral components, whose relative weights shift as the membrane mimetic moves from detergent micelles toward bilayers with increasing amounts of cholesterol. The different spectral components are highlighted in gray. The darker gray box indicates a broader, more immobilized component (I) that increases in intensity from top to bottom in Figure 2. The more mobile component (M) indicated by a lighter gray box decreases in intensity from top to bottom.

Considering the impact that cholesterol has on the ability of M2 to initiate viral budding, we were particularly intrigued by the differences seen in the EPR line shapes in POPC/POPG bilayers upon the addition of cholesterol (Figure 2). We thus designed experiments to more fully characterize cholesterol-induced change in M2 conformation and dynamics.

Line Shapes for Sites within the C-Terminal Domain Are a Weighted Average of Two Different Components. In Figure 2, one spin-labeled site (I42C) is used to analyze the impact of the environment on line shape. In Figure 3, we show EPR spectra for five different sites located before and within the

DOI: 10.1021/acs.biochem.5b01065
Biochemistry 2015, 54, 7157−7167

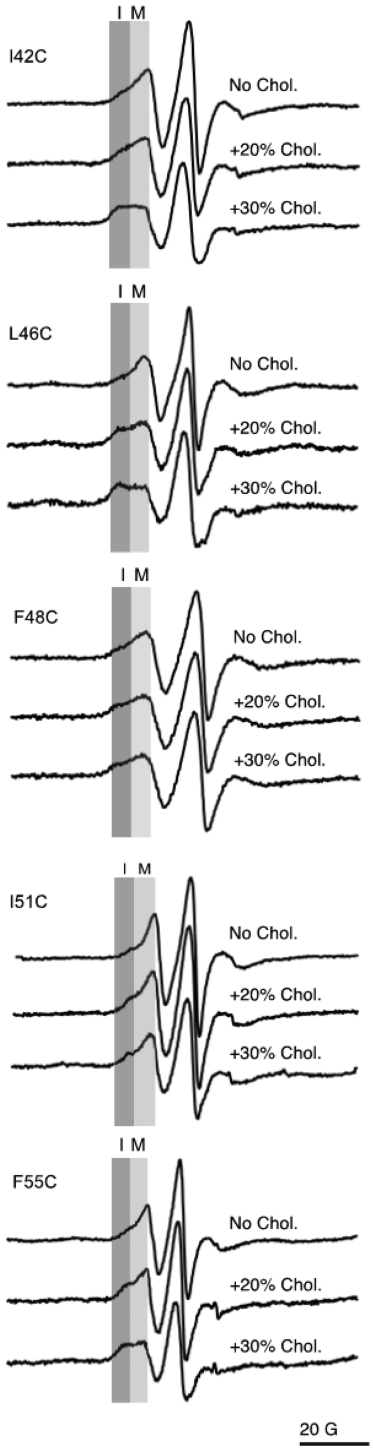

Figure 3. Normalized X-band CW EPR spectra of M2TMC (23−60) spin-labeled at sites I42C, L46C, F48C, I51C, and F55C in POPC/POPG 4:1 bilayers in the absence and presence of cholesterol. Each sample was spin-diluted with unlabeled peptide (unlabeled/labeled 4:1) to eliminate broadening resulting from spin-coupling between monomers within the homotetrameric protein. The light gray box (M) and dark gray box (I) refer to the peak corresponding to the mobile and immobile conformations, respectively.

C-terminal amphipathic helix. The goal of this experiment was to rule out the possibility that the two-component nature of the M2TMC-I42SL spectra shown in Figure 2 was simply a localized effect for site 42.

As demonstrated in Figure 3, the EPR spectra for all five sites exhibit a two-component nature. The two components present are labeled as mobile (M) and immobile (I). As the cholesterol content of the lipid bilayer changes, the relative intensities of these two components change. With increasing cholesterol concentration, the peak corresponding to the more immobile component increases in intensity as this conformation becomes more populated. The observation that this trend is seen for all five sites is consistent with a concerted cholesterol-dependent change occurring in this region.

Shown in Figure 4A are EPR spectra for site 55 and fits using an EPR simulation package based on the MOMD approach[30]

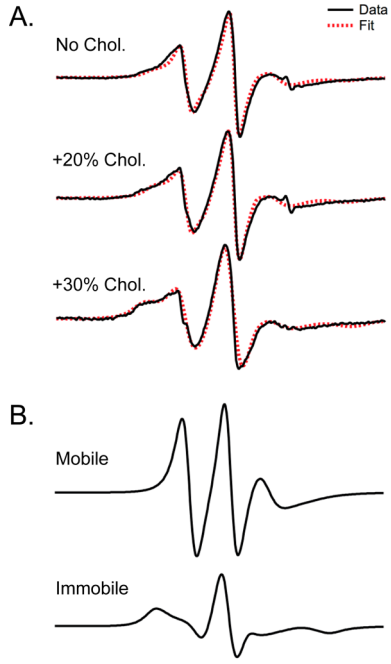

Figure 4. Simulation of line shapes for different amounts of cholesterol indicate a good fit to experimental data can be achieved using a weighted average of two different spectral components. (A) EPR spectra for M2TMC spin-labeled at site F55C in POPC/POPG (4:1) bilayers with varying amounts of cholesterol (black lines) along with simulations (red dashed lines). (B) Spectra corresponding to the mobile and immobile components used to fit lineshapes. The mobile and immobile components have correlation times of 2.43 and 8.55 ns, respectively. In the cholesterol-free, 20% cholesterol, and 30% cholesterol environments, the relative population of the immobile component is 45, 57, and 68%, respectively.

(see Materials and Methods for details). Simulations of these spectra required two motional components to obtain a reasonable fit, but they were not improved by including a third motional component. The mobile and immobile components have correlation times of 2.43 and 8.55 ns, respectively. In the cholesterol-free, 20% cholesterol, and 30% cholesterol environments, the relative population of the immobile component is 45, 57, and 68%, respectively.

The work presented in this article uses a M2 construct (M2TMC 23−60) that does not include the last 37 residues of the C-terminal domain. It is conceivable that the multicomponent nature of the EPR line shapes seen in Figures 2 and 3 could be attributed to the use of a truncation of the full-length protein. However, it has recently been demonstrated that the multicomponent EPR line shapes we observe for sites within

DOI: 10.1021/acs.biochem.5b01065
Biochemistry 2015, 54, 7157−7167

the amphipathic helix of M2 are very similar to the line shapes observed for the same sites on the full-length M2 protein.[21] The secondary structure and membrane depth of the amphipathic helix in M2TMC 23−60 is also strikingly similar to the same region in the full-length M2 protein.[21] These findings suggest that the multicomponent nature we report here is an intrinsic property of the M2 protein.

Saturation Recovery Data Are Consistent with Conformational Exchange of C-Terminal Amphipathic Helix. The two-component EPR spectra shown in Figure 3 can arise from an equilibrium involving either different conformational substates of the M2 protein or different rotamers of the MTSL spin-label.[19] It is important to be able to distinguish between the origins of multicomponent line shapes, and the SR-EPR technique is well-suited for this measurement.[19] In SR-EPR, an intense saturation pulse is delivered at a frequency corresponding to the central line of the nitroxide. The return of spectral intensity is monitored with a weak CW observing microwave field at the same frequency and occurs with a characteristic time constant, T_1. For a system with spin-label rotameric exchange in the absence of conformational exchange, a single-exponential recovery is expected. For a system undergoing conformational exchange, the relaxation to equilibrium is generally biexponential with relaxation rate constants that are a function of the intrinsic T_1 values of the two components and the exchange rate. Rotamer exchange for a MTSL spin-label lies on the ∼0.1−1 μs time scale range, whereas conformational exchange is at least an order of magnitude slower.[19]

SR-EPR data were collected for sites 42, 51, and 55. SR-EPR data for site 55 are presented in Figure 5. As shown in Figure 5, the saturation recovery curve for site 55 is best fit by a double exponential, which corresponds to two unique spin−lattice relaxation rates, consistent with conformational exchange. SR-EPR data for sites 42 and 51 (Figure S1) are also characterized by double-exponential recoveries. The observation of double-exponential recoveries for all three sites (42, 51, and 55) is consistent with conformational exchange of the entire C-terminal amphipathic helix and not with localized effects at a single residue.

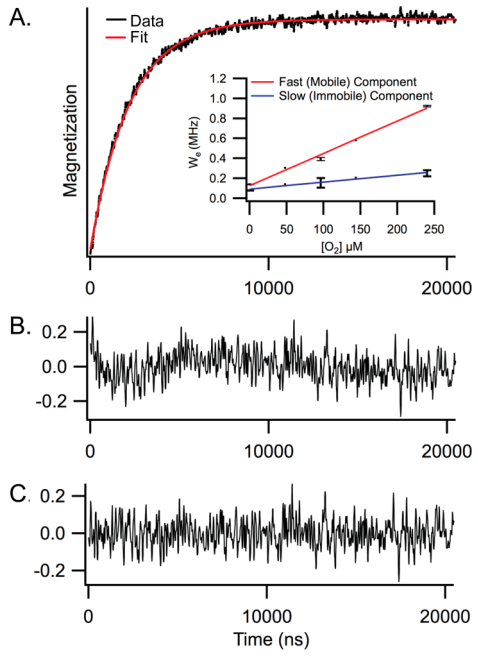

Figure 5. Saturation-recovery data indicate two components in conformational exchange. (A) Representative saturation curve for M2TMC spin-labeled at site F55C in POPC/POPG (4:1) under 20% air (black) with a double-exponential fit (red). Inset shows the dependence of the spin−lattice relaxation rates on the concentration of oxygen for the fast, mobile (red) and slow, immobile (blue) saturation-recovery components. (B) Residual of a single-exponential fit. (C) Residual of a double-exponential fit.

Spin-labels in two different conformational states can have different accessibilities to paramagnetic relaxation agents (such as oxygen) that will modulate the intrinsic T_1 values of the two states. O_2 is a hydrophobic molecule and preferentially partitions into lipid bilayers, with the highest concentration of O_2 in the middle of the bilayer. Figure 5A (inset) shows the dependence of the spin−lattice relaxation rates on the concentration of oxygen. The data shown indicate the slow component (blue line) is less dependent on changes in oxygen concentration than the fast component (red line), which is consistent with the slow component being less accessible to oxygen and thus not as deep in the hydrophobic membrane. The finding that the less mobile component is less deeply buried in the membrane may at first seem surprising. For many membrane proteins, regions that are more deeply buried in the membrane are immobilized relative to regions that are on the surface of the membrane.[18] However, as we will discuss below, both protein−protein interactions and cholesterol binding are also means for immobilization of the M2 protein.

Accessibility Studies Show That the Conformational State of the C-Terminal Helix That Becomes More Populated upon the Addition of Cholesterol Is Not as Deep in the Membrane as the Other Conformation. The saturation recovery data described above indicate that the two conformations of the C-terminal helix of M2 have different accessibilities to membrane-soluble paramagnetic oxygen. To further explore this finding, we used another complementary method that also probes membrane accessibility (power saturation) and collected data for four sites within the C-terminal amphipathic helix (46, 48, 51, and 55).

Power saturation EPR experiments have been widely used in SDSL-EPR to determine a residue's accessibility to paramagnetic reagents.[42] In our experiments, accessibility to two paramagnetic reagents, NiEDDA and O_2, were measured by probing changes in the relaxation efficiency of the spin-label in the presence of these compounds. As mentioned above, O_2 is a hydrophobic molecule that preferentially partitions into lipid bilayers. Conversely, NiEDDA is a hydrophilic compound that remains in the aqueous phase. Accessibility to NiEDDA and O_2 provide complementary data, and, as such, the trends seen should be self-consistent.

All of the sites within the amphipathic helix (46, 48, 51, and 55) have increased accessibility to NiEDDA (Figure 6A) and decreased accessibility to oxygen (Figure 6B) upon addition of cholesterol. The data are consistent with the amphipathic helix becoming less buried in the membrane upon addition of cholesterol. Although we can say with confidence that the helix is on average deeper in the membrane in the absence of cholesterol, there are significant challenges to assigning specific distances to the changes in membrane depths. The power saturation studies report on data from both conformational states present. Reporting quantitative distances near the membrane surface for our membrane-bound M2 protein is complicated by a lack of distance calibration points above the

DOI: 10.1021/acs.biochem.5b01065
Biochemistry 2015, 54, 7157−7167

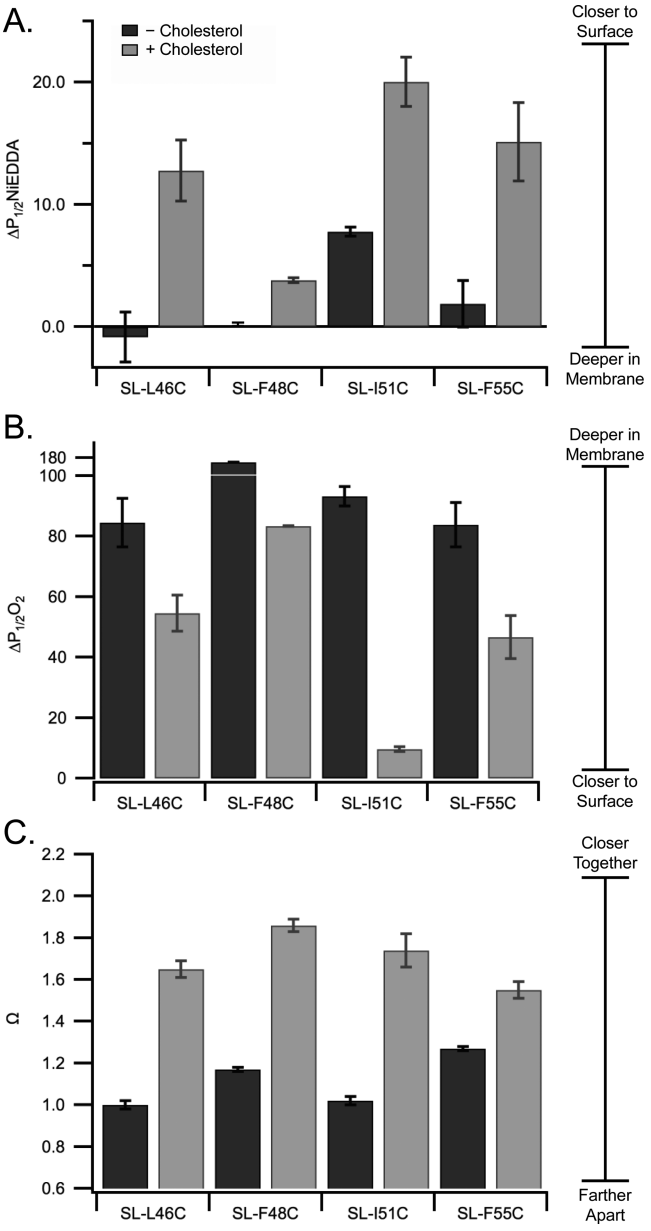

Figure 6. Addition of cholesterol changes the membrane topology of the C-terminal juxtamembrane region. Accessibility data to NiEDDA (A) and oxygen (B) and interaction parameter (Ω) data (C) for M2TMC labeled at the indicated sites in POPC/POPG (4:1) bilayers with 0 and 30% cholesterol. Ω is the ratio of the central line intensity for fully labeled and spin-diluted samples. Spectra used to calculate Ω are shown in Figure S2.

glycerol backbone.[43] Therefore, we do not report a quantitative change in depth due to these limitations. We can say, however, that the changes in oxygen accessibility we observe here are substantially larger than what was reported for changes in oxygen accessibility for the M2 C-terminal amphipathic helix resulting from pH-triggered opening of the M2 proton channel.[13]

Studies on other proteins have demonstrated that cholesterol addition to membranes decreases the ability of membrane-associating helices to penetrate into the lipid headgroup region.[44−46] As explained in more detail in the Discussion, we postulate that the observed movement of the amphipathic helices away from the membrane surface could result from the condensing effect cholesterol induces on liquid-disordered phases, which decreases the ability of membrane-associating helices to penetrate into the lipid headgroup region.[47]

Distance-Dependent Dipolar Couplings Demonstrate That the C-Terminal Amphipathic Helix Is More Closely Packed in the Presence of Cholesterol. The data presented in Figure 6A,B clearly demonstrate that the C-terminal amphipathic helix of M2 changes in membrane depth upon the addition of cholesterol. We next explored whether there was a change in the arrangement of the C-terminal amphipathic helices within the homotetramer upon the addition of cholesterol. These experiments would also be a test of the hypothesis that increased intersubunit interactions between the amphipathic helices might account for our observed immobilization of M2 in the presence of cholesterol.

Broadening of CW-X-band line shapes is observed when two spin-labels are less than ∼20 Å apart.[42] Dipolar coupling leads to peak broadening and a decrease in the central peak intensity. It is possible to quantify dipolar coupling by comparing central peak intensities between a fully labeled sample, which has four spin-labeled M2 monomers per tetramer, and a dilute labeled sample, which has only one spin-labeled M2 monomer per tetramer. An Ω value greater than 1 indicates that there is significant broadening due to dipolar coupling of sites separated by less than ∼20 Å. Since CW EPR gives an averaged spectrum, Ω reflects the effect of dipolar coupling for both M2 C-terminal conformational states.

Ω values are shown in Figure 6C for M2 both with and without cholesterol. The addition of cholesterol increases the measured value of Ω for all four sites. Ω values result from dipolar coupling, which is inversely proportional to interlabel distance. Thus, the measured increases in Ω values for sites 46, 48, 51, and 55 indicate the addition of cholesterol leads to the closer approach of M2 subunits within the tetrameric bundle.

It is challenging to quantitatively interpret Ω values for this system. Our measured Ω values reflect dipolar coupling from both conformational states present, which have overlapping central peaks. It is nontrivial to extract reliable quantitative distances from dipolar broadened CW line shapes when more than one conformation is present.[18,48]

DEER Data Reveal Distances Consistent with More than One Conformation. DEER EPR can resolve distance distributions within a population as well as measure distances longer than the ∼20 Å limit measurable from broadening of CW line shapes.[49,50] Furthermore, DEER has been successfully applied to membrane proteins,[29,51] although resolving distances in homo-oligomeric proteins has proven to be challenging.[37] For example, a single labeled site in a homotetramic protein with a single conformation would lead to two measurable distances, one resulting from subunits that are next to each other within the tetrameric bundle (proximal) and another distance resulting from monomers that are diagonally related across the tetrameric bundle (Figure S3). With two distinct conformations of a homotetramer, we thus theoretically expect four unique distances (Figure S3).

DEER data for sites 51 and 55 are shown in Figure 7, with corresponding L-curves shown in Figure S4. A model-free Tikhonov regularization fit was used to determine an approximate distance distribution.[35] The Tikhonov regularization of site 51 (λ = 40) reveals local maxima at approximately 24, 31, and 40 Å. The Tikhonov regularization of site 55 (λ = 25) reveals local maxima at approximately 19, 33, 37, and 47 Å. The distance distributions shown in Figure 7 include more than

DOI: 10.1021/acs.biochem.5b01065
Biochemistry 2015, 54, 7157−7167

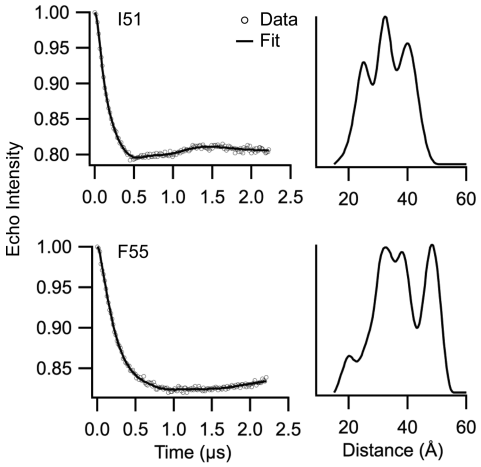

Figure 7. DEER reveals presence of multiple distances and protein conformations. Tikhonov regularization and distance distributions of M2TMC-I51C (λ = 40, top) and M2TMC-F55C (λ = 25, bottom). Background-subtracted DEER data are shown as open circles, and corresponding fits, as black lines. L-curves are shown in Figure S4. M2 peptides were incorporated into 1,2-dihexanoyl-*sn*-glycero-3-phosphocholine (DHPC) at a peptide/DHPC molar ratio of 1:500.

the two distances predicted for a single conformation of a homotetramer and are consistent with the presence of more than one conformation. However, our time domain data does not show particularly well-defined oscillations, which suggests that we should interpret the data with caution.

The reliability of our distance distributions is supported by analyses of both sites 51 and 55 in different hydrophobic environments. Distance distributions for each of these two sites reveal local maxima at similar distances regardless of the membrane mimic employed to solubilize the protein. (Figure S5). Although there are similarities between the unique DEER distances, there are significant differences in the intensities of the peaks. This indicates that the multiple distances observed in Figure 7 likely correspond to unique protein conformations that are not artifacts of data analysis or a particular hydrophobic environment but that exist in different membrane mimics with varying populations.

It is instructive to compare the distances shown in Figure 7 to published models for M2. Published models that used a M2 construct similar to the M2 peptide employed in this article include a model based on solid-state NMR (ssNMR) in bilayers consisting of 1,2-dioleoyl-*sn*-glycero-3-phosphocholine (DOPC) and 1,2-dioleoyl-*sn*-glycero-3-phosphoethanolamine (DOPE), DOPC/DOPE 4:1 (PDB 2L0J),[40] and a model based on solution-state NMR in DHPC micelles (PDB: 2RLF).[26] DEER-derived distances for both I51 and F55 are similar to some of the distances measured from the ssNMR model collected in DOPC/DOPE lipid bilayers (Figure S6).[40] Distances were measured between $H_{C,\gamma}$ of corresponding sites from the published ssNMR model (PDB 2L0J).

The DEER data for site 51 includes a distance at ∼24 Å, which is similar to the diagonal distance between $H_{C,\gamma}$ (∼24 Å) observed in the ssNMR model of M2 in bilayers.[40] The proximal distance for this conformation (∼17 Å) would not be observed in the DEER data because it is below the ∼20 Å detection limit of the method. The DEER distances for site 51 at ∼31 and 40 Å likely correspond to the proximal and diagonal distances of a previously uncharacterized less packed conformational state. The ∼31 and 40 Å DEER distances have a ratio close to 1:1.4, which is expected from the proximal/diagonal distances in a symmetric homotetramer.

The DEER data for site 55 includes a distance at ∼19 Å, which is similar to the diagonal distance between $H_{C,\gamma}$ (∼19 Å) observed in the ssNMR model of M2 in bilayers.[40] The proximal distance for site 55 for this conformation (∼15 Å) would not be observed in the DEER data because it is below the ∼20 Å detection limit of the method. The site 55 DEER distances of ∼33 and 47 Å have a ratio of 1:1.4. These two distances could correspond to the proximal and diagonal distances of a previously uncharacterized less packed conformational state. The fact that the existence of these pairs of distances for both sites 51 and 55 do not correspond to distances in previously published structures provides strong evidence that these longer distances are from one of two conformational states that we have detected using line shape analysis and saturation recovery.

The proximal and diagonal distances measured from the M2 model in micelles[26] are 12 and 16.5 Å for I51 and 4.7 and 7.3 Å for F55, respectively. All four of these distances are below the ∼20 Å detection limit of DEER. However, a recent solution NMR study compared the model of M2 in DHPC micelles to M2 in DMPC/DHPC bicelles,[14] and unlike the micelle model, the bicelle structure has significant similarities with the published ssNMR structure in bilayers.

DISCUSSION

Data from line shape analyses, relaxation rates, accessibility parameters, and the measurement of distance-dependent dipolar couplings provide rich complementary information on the conformations of the C-terminal amphipathic helix of M2 protein. We have been able to demonstrate that the C-terminal amphipathic helix populates at least two conformations in POPC/POPG 4:1 bilayers, a lipid environment in which M2-induced functional budding assays have been carried out.[8] Furthermore, we have been able to show that the conformational state of the C-terminal amphipathic helix that becomes more populated in the presence of cholesterol is less dynamic, less membrane buried, and more tightly packed than the other state. As described below, the intriguing result that the conformation that is less membrane buried is also less mobile could be attributed to the changes cholesterol induces in bilayer properties and/or direct binding of cholesterol to the protein.

M2 Protein as a "Shape Shifter". The hypothesis that the M2 protein has multiple low-energy conformational states is not new.[23,52−58] It has been suggested that the various structural models proposed to date provide snapshots of distinct conformational states sampled by the protein during the viral life cycle. The M2 protein has at least two functions, the proton channel activity crucial for uncoating of virions[9] and the generation of curvature essential for viral budding.[10] These two distinct functions could conceivably require two different conformations.

Several studies have specifically addressed the potential for the C-terminal amphipathic helices of M2 to adopt different conformations. An early paper postulated that the C-terminal region might adopt either a water-soluble helical extension of the transmembrane helix or that each amphipathic helix of the extension could individually make a tight, 90° turn and then bind hydrophobically to the membrane.[57] SDSL-EPR data has demonstrated that the C-terminal amphipathic helix of M2 in POPC/POPG 4:1 lipid bilayers lies on the membrane surface but that it changes in membrane depth and helix packing in

DOI: 10.1021/acs.biochem.5b01065
Biochemistry 2015, 54, 7157−7167

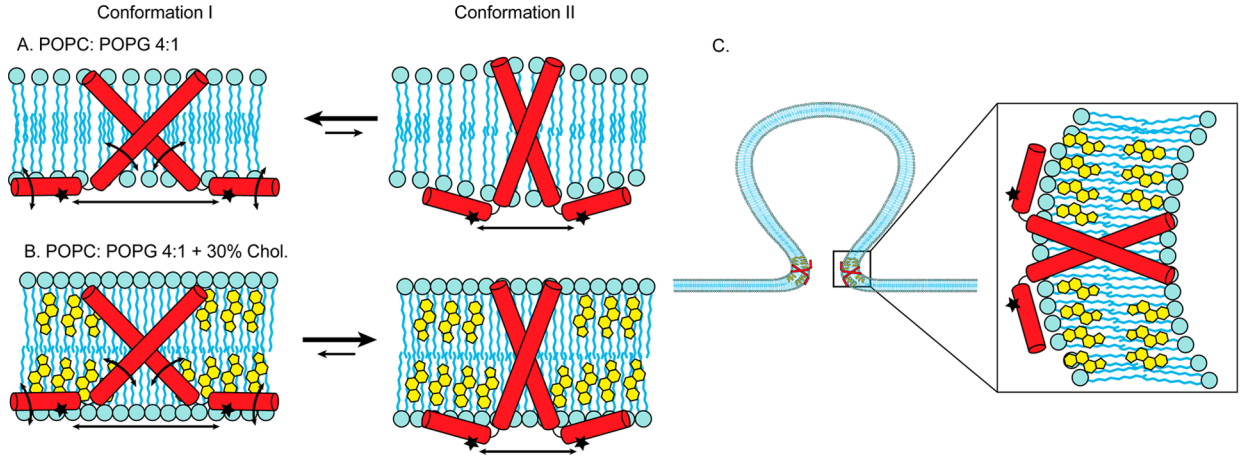

Figure 8. Cartoon model that is consistent with experimental data collected on the C-terminal amphipathic helices of M2: Conformation I (left in panels A and B) and Conformation II (right in panels A and B). As compared to Conformation I, the C-terminal helices of Conformation II are less mobile, less deep in the membrane, and closer together within the homotetramer. (A) In the absence of cholesterol, both Conformation I and Conformation II are present, but the equilibrium is shifted toward Conformation I. (B) In the presence of cholesterol, both Conformation I and Conformation II are present, but cholesterol preferentially stabilizes Conformation II and the equilibrium is shifted toward Conformation II. (C) We postulate that in the highly curved region of the neck of viral budding where cholesterol is concentrated Conformation II is predominant. For clarity, only two of the four subunits of a M2 homotetramer are shown in the cartoon models.

response to pH,[13] the addition of adamantane drugs,[20] and the lipid composition of the bilayer.[22] Solution NMR work has shown that the conformation of the C-terminal amphipathic helix changes depending on solubilizing conditions and that models based on data from DHPC micelles[26] differ from models based on data collected in DMPC/DHPC bicelles.[14] ssNMR studies have also shown that the conformation of the M2 protein changes depending on the composition of the bilayer.[58]

Characteristics of M2 That Promote Conformational Exchange. The inherent flexibility that allows M2 to access multiple conformational states was predicted by the observation that a remarkably large fraction of M2 variants with mutations at the transmembrane helix–helix interfaces maintains the ability of the protein to tetramerize.[54] The ability of the M2 protein to tolerate mutations along the helix–helix interfaces is consistent with structural plasticity that may be required for functional requirements for conformational exchange.

Beyond M2, it has been observed that stabilizing interactions have gone untapped in many other transmembrane proteins.[59] The lack of stability optimization has been hypothesized to result from the fact that the surrounding lipid bilayer provides enough constraints on membrane proteins for sufficient stability for cell viability. Furthermore, flexibility of membrane proteins could facilitate exchange between different states critical to the function of many membrane proteins, including proteins that act as gated channels and receptors that transduce signals across membranes.[60] SDSL-EPR has been demonstrated to be particularly well-suited to detect conformational substates of membrane proteins.[61]

In addition to the inherent plasticity in the packing of the four helices in the transmembrane domain in M2, it is likely that the loop region between the transmembrane domain and C-terminal domain could act as a flexible hinge. Movement about this flexible hinge could allow for different packing arrangements and different membrane depths of the four C-terminal amphipathic helices.

Model for How Cholesterol Leads to the Conformational Shift Seen in Our EPR Data. The impact of cholesterol on the M2 protein could be due to changes cholesterol induces in the lipids surrounding the protein, direct binding of cholesterol to the protein, or a combination of both effects. Cholesterol is a polycyclic amphipathic molecule.[62] The apolar section of cholesterol buried in the membrane has an asymmetric structure with two distinct faces that could form numerous van der Waals interactions with either lipids or membrane associated proteins. The polar section of cholesterol is a single hydroxyl (OH), which could form a hydrogen bond with either a lipid or membrane-associated protein.

Cholesterol can have a range of impacts on lipid bilayer properties depending of the lipid composition of the membrane and the temperature.[63] The POPC/POPG 4:1 lipid bilayers used in this study are in the liquid-disordered phase at room temperature.[64] Cholesterol exerts a condensing effect on liquid-disordered phases and increases the thickness of the bilayer.[47] It has been previously demonstrated that increasing the thickness of the bilayer decreases the tilt of helices within the transmembrane domain of M2, leading to a more tightly packed homotetramer.[23] A number of studies have also shown that the condensing effect of cholesterol on membranes decreases the ability of membrane-associating helices to penetrate into the lipid headgroup region.[44−46] This effect could explain our finding that the C-terminal amphipathic helix of M2 moves away from the membrane surface upon the addition of cholesterol.

Cholesterol binding has been characterized for a range of different membrane proteins.[65−67] The observation that M2 localizes to the edge the cholesterol-rich budozone on the surface of an infected cell has been pointed to as evidence that there is a cholesterol binding site on the M2 protein.[24] The M2 protein contains a possible cholesterol recognition/interaction amino acid consensus (CRAC) sequence,[8,24] but the looseness of the CRAC definition ((L/V)-X_{1-5}-(Y)-X_{1-5}-(K/R)) has raised some skepticism about its predictive value.[66] However, in the case of M2, the observation that the removal of a mandatory tyrosine within the proposed CRAC domain of M2 disrupts the association of the M2 protein with cholesterol-

DOI: 10.1021/acs.biochem.5b01065
Biochemistry 2015, 54, 7157−7167

containing membrane surfaces lends support to the existence of a cholesterol binding site.[68]

The direct binding of cholesterol to M2 could explain why the addition of cholesterol shifts the conformational equilibrium toward a more immobilized state. The pairing of a transmembrane helix surface with a rigid cholesterol molecule could be expected to be entropically advantageous compared with association with more flexible lipids.[67] It has also been previously suggested for other membrane proteins that the apolar faces of cholesterol could interact with neighboring transmembrane domains and exert a condensing effect on the whole protein.[62] This cholesterol-induced condensing effect could not only account for the observed immobilization but also explain the observed closer approach of the C-terminal helices within the tetrameric bundle.

A postulated model that incorporates our experimental data into the two observed conformations of M2 is shown in Figure 8. As compared to Conformation I (left in Figure 8A,B), the C-terminal helices of Conformation II (right in Figure 8A,B), are less mobile, less deep in the membrane, and closer together within the homotetramer. In the absence of cholesterol, both Conformation I and Conformation II are present, but the equilibrium is shifted toward Conformation I. In the presence of cholesterol, both Conformation I and Conformation II are present, but cholesterol preferentially stabilizes Conformation II and the equilibrium is shifted toward Conformation II. Therefore, we postulate that Conformation II is predominant in the highly curved region of the neck of viral budding where cholesterol is concentrated (Figure 8C). The fact that viral budding is cholesterol-dependent supports our proposal that Conformation II is relevant for budding. Furthermore, observations from DEER data with membrane mimics containing different degrees of curvature (Figure S5) indicate samples with less curved bilayered membranes include substantially longer distances representative of Conformation I compared to samples with highly curved membrane mimics (micelles and bicelles).[27]

SUMMARY AND CONCLUSIONS

The C-terminal amphipathic helix of the influenza A M2 protein plays a critical cholesterol-dependent role in viral budding. In principle, a detailed understanding of M2-mediated viral budding could assist in the development of antiviral drugs targeted to influenza. With the goal of providing atomic-level details on the role cholesterol plays in budding, we spin- labeled sites right before and within the C-terminal amphipathic helix of the M2 protein and studied the proteins in membranes both with and without cholesterol. We used a multipronged SDSL-EPR approach and collected data on line shapes, relaxation rates, accessibility of residues to the membrane, and distances between symmetry-related sites within the tetrameric protein. Our results demonstrate the existence of two conformational states of the C-terminal amphipathic helix that differ in mobility, subunit arrangement, and membrane depth. The condensing effect cholesterol exerts on lipid bilayers and/or direct binding of cholesterol to M2 could help to explain the observed shift in the populations of conformational states upon the addition of cholesterol and suggests that the predominant conformation we observe in the presence of cholesterol is relevant for the understanding of viral budding.

ASSOCIATED CONTENT

Supporting Information

The Supporting Information is available free of charge on the ACS Publications website at DOI: 10.1021/acs.biochem.5b01065.

Representative saturation recovery traces for M2TMC-I42C and M2TMC-I51C in POPC/POPG; CW-EPR spectra of five mutants of M2TMC in POPC/POPG bilayers in the absence and presence of cholesterol; hypothetical DEER distance distributions for a spin-labeled homotetrameric protein; Tikhonov L-curve for M2TMC-I51C and M2TMC-F55C for DEER data shown in Figure 7; Tikhonov regularization and distance distributions of M2TMC-I51C in bicelles and Lipodisqs and M2TMC-F55C in Lipodisq as well as their overlays; comparison of ssNMR model (PDB 2L0J) with experimental DEER data (PDF)

AUTHOR INFORMATION

Corresponding Author

*E-mail: khoward1@swarthmore.edu.

Funding

This work was generously supported by the National Institutes of Health AI094483 (to K.P.H.). The National Biomedical EPR Center is supported by P41 EB001980. The research was also supported by NIH R01 GM108026, NSF CHE-1011909, and NSF MRI-0722403 (to G.A.L.).

Notes

The authors declare no competing financial interest.

ACKNOWLEDGMENTS

We would like to thank long-term M2 collaborator Bill DeGrado and his postdoctoral fellow Dr. Jun Wang for synthesis of the M2 peptides.

ABBREVIATIONS

SDSL-EPR, site-directed spin labeling electron paramagnetic resonance; CW-EPR, continuous wave electron paramagnetic resonance; SR-EPR, saturation-recovery EPR; DEER, double electron−electron resonance; MTSL, 1-oxyl-2,2,5,5-tetramethylpyrro-3-methylmethanethiosulfonate; POPC, 1-palmitoyl-2-oleyl-*sn*-glycero-phosphocholine; POPG, 1-palmitoyl-2-oleyl-*sn*-glycero-3-[phospho-*rac*-(1-glycerol)]; DHPC, 1,2-dihexanoyl-*sn*-glycero-3-phosphocholine; MOMD, microscopic order macroscopic disorder; ssNMR, solid-state NMR; NiEDDA, nickel(II) ethylenediaminediacetate

REFERENCES

(1) de la Barrera, C., and Reyes-Teran, G. (2005) Influenza: Forecast for a pandemic. *Arch. Med. Res. 36*, 628−636.

(2) Fukuyama, S., and Kawaoka, Y. (2011) The pathogenesis of influenza virus infections: the contributions of virus and host factors. *Curr. Opin. Immunol. 23*, 481−486.

(3) Krug, R. M., and Aramini, J. M. (2009) Emerging antiviral targets for influenza A virus. *Trends Pharmacol. Sci. 30*, 269−277.

(4) Rossman, J. S., Jing, X. H., Leser, G. P., Balannik, V., Pinto, L. H., and Lamb, R. A. (2010) Influenza Virus M2 Ion Channel Protein Is Necessary for Filamentous Virion Formation. *J. Virol. 84*, 5078−5088.

(5) Stewart, S. M., and Pekosz, A. (2011) Mutations in the membrane-proximal region of the influenza A virus M2 protein cytoplasmic tail have modest effects on virus replication. *J. Virol. 85*, 12179−12187.

DOI: 10.1021/acs.biochem.5b01065
Biochemistry 2015, 54, 7157−7167

(6) Roberts, K. L., Leser, G. P., Ma, C. L., and Lamb, R. A. (2013) The Amphipathic Helix of Influenza A Virus M2 Protein Is Required for Filamentous Bud Formation and Scission of Filamentous and Spherical Particles. *J. Virol. 87*, 9973−9982.
(7) Rossman, J. S., and Lamb, R. A. (2013) Viral membrane scission. *Annu. Rev. Cell Dev. Biol. 29*, 551−569.
(8) Rossman, J. S., Jing, X., Leser, G. P., and Lamb, R. A. (2010) Influenza virus M2 protein mediates ESCRT-independent membrane scission. *Cell 142*, 902−913.
(9) Pinto, L. H., and Lamb, R. A. (2006) The M2 proton channels of influenza A and B viruses. *J. Biol. Chem. 281*, 8997−9000.
(10) Rossman, J. S., and Lamb, R. A. (2011) Influenza virus assembly and budding. *Virology 411*, 229−236.
(11) Iwatsuki-Horimoto, K., Horimoto, T., Noda, T., Kiso, M., Maeda, J., Watanabe, S., Muramoto, Y., Fujii, K., and Kawaoka, Y. (2006) The cytoplasmic tail of the influenza A virus M2 protein plays a role in viral assembly. *J. Virol. 80*, 5233−5240.
(12) Chen, B. J., Leser, G. P., Jackson, D., and Lamb, R. A. (2008) The influenza virus M2 protein cytoplasmic tail interacts with the M1 protein and influences virus assembly at the site of virus budding. *J. Virol. 82*, 10059−10070.
(13) Nguyen, P. A., Soto, C. S., Polishchuk, A., Caputo, G. A., Tatko, C. D., Ma, C. L., Ohigashi, Y., Pinto, L. H., DeGrado, W. F., and Howard, K. P. (2008) pH-induced conformational change of the influenza M2 protein C-terminal domain. *Biochemistry 47*, 9934−9936.
(14) Claridge, J. K., Aittoniemi, J., Cooper, D. M., and Schnell, J. R. (2013) Isotropic Bicelles Stabilize the Juxtamembrane Region of the Influenza M2 Protein for Solution NMR Studies. *Biochemistry 52*, 8420−8429.
(15) Drin, G., and Antonny, B. (2010) Amphipathic helices and membrane curvature. *FEBS Lett. 584*, 1840−1847.
(16) Shen, H., Pirruccello, M., and De Camilli, P. (2012) SnapShot: Membrane Curvature Sensors and Generators. *Cell 150*, 1300−U1226.
(17) Jensen, M. B., Bhatia, V. K., Jao, C. C., Rasmussen, J. E., Pedersen, S. L., Jensen, K. J., Langen, R., and Stamou, D. (2011) Membrane Curvature Sensing by Amphipathic Helices, a single liposome study using alpha synuclein and annexin B12. *J. Biol. Chem. 286*, 42603−42614.
(18) Bordignon, E. (2011) Site-Directed Spin Labeling of Membrane Proteins. *Top. Curr. Chem. 321*, 121−157.
(19) Bridges, M., Hideg, K., and Hubbell, W. (2010) Resolving Conformational and Rotameric Exchange in Spin-Labeled Proteins Using Saturation Recovery EPR. *Appl. Magn. Reson. 37*, 363−390.
(20) Thomaston, J. L., Nguyen, P. A., Brown, E. C., Upshur, M. A., Wang, J., Degrado, W. F., and Howard, K. P. (2013) Detection of drug-induced conformational change of a transmembrane protein in lipid bilayers using site-directed spin labeling. *Protein Sci. 22*, 65−73.
(21) Huang, S., Green, B., Thompson, M., Chen, R., Thomaston, J., DeGrado, W. F., and Howard, K. P. (2015) C-terminal juxtamembrane region of full-length M2 protein forms a membrane surface associated amphipathic helix. *Protein Sci. 24*, 426−429.
(22) Saotome, K., Duong-Ly, K. C., and Howard, K. P. (2015) Influenza A M2 protein conformation depends on choice of model membrane. *Biopolymers 104* (4), 405−411.
(23) Duong-Ly, K. C., Nanda, V., Degrad, W. F., and Howard, K. P. (2005) The conformation of the pore region of the M2 proton channel depends on lipid bilayer environment. *Protein Sci. 14*, 856−861.
(24) Schroeder, C., Heider, H., Moncke-Buchner, E., and Lin, T. (2005) The influenza virus ion channel and maturation cofactor M2 is a cholesterol-binding protein. *Eur. Biophys. J. 34*, 52−66.
(25) Thaa, B., Siche, S., Herrmann, A., and Veit, M. (2014) Acylation and cholesterol binding are not required for targeting of influenza A virus M2 protein to the hemagglutinin-defined budozone. *FEBS Lett. 588*, 1031−1036.
(26) Schnell, J. R., and Chou, J. J. (2008) Structure and mechanism of the M2 proton channel of influenza A virus. *Nature 451*, 591−595.
(27) Wang, T., and Hong, M. (2015) Investigation of the Curvature Induction and Membrane Localization of the Influenza Virus M2 Protein Using Static and Off-Magic-Angle Spinning Solid-State Nuclear Magnetic Resonance of Oriented Bicelles. *Biochemistry 54*, 2214−2226.
(28) Schmidt, N. W., Mishra, A., Wang, J., DeGrado, W. F., and Wong, G. C. L. (2013) Influenza Virus A M2 Protein Generates Negative Gaussian Membrane Curvature Necessary for Budding and Scission. *J. Am. Chem. Soc. 135*, 13710−13719.
(29) Sahu, I. D., McCarrick, R. M., Troxel, K. R., Zhang, R. F., Smith, H. J., Dunagan, M. M., Swartz, M. S., Rajan, P. V., Kroncke, B. M., Sanders, C. R., and Lorigan, G. A. (2013) DEER EPR Measurements for Membrane Protein Structures via Bifunctional Spin Labels and Lipodisq Nanoparticles. *Biochemistry 52*, 6627−6632.
(30) Budil, D. E., Lee, S., Saxena, S., and Freed, J. H. (1996) Nonlinear-least-squares analysis of slow-motion EPR spectra in one and two dimensions using a modified Levenberg-Marquardt algorithm. *J. Magn. Reson., Ser. A 120*, 155−189.
(31) Kroncke, B., Horanyi, P., and Columbus, L. (2010) Structural Origins of Nitroxide Side Chain Dynamics on Membrane Protein alpha-Helical Sites. *Biochemistry 49*, 10045−10060.
(32) Yin, J., Feix, J., and Hyde, J. (1990) Mapping of collision frequencies for stearic-acid spin labels by saturation-recovery electron-paramagnetic resonance. *Biophys. J. 58*, 713−720.
(33) Pyka, J., Ilnicki, J., Altenbach, C., Hubbell, W., and Froncisz, W. (2005) Accessibility and dynamics of nitroxide side chains in T4 lysozyme measured by saturation recovery EPR. *Biophys. J. 89*, 2059−2068.
(34) Jeschke, G. (2012) DEER Distance Measurements on Proteins. *Annu. Rev. Phys. Chem. 63*, 419−446.
(35) Jeschke, G., Chechik, V., Ionita, P., Godt, A., Zimmermann, H., Banham, J., Timmel, C. R., Hilger, D., and Jung, H. (2006) DeerAnalysis2006 - a comprehensive software package for analyzing pulsed ELDOR data. *Appl. Magn. Reson. 30*, 473−498.
(36) Chiang, Y., Borbat, P., and Freed, J. (2005) The determination of pair distance distributions by pulsed ESR using Tikhonov regularization. *J. Magn. Reson. 172*, 279−295.
(37) Dalmas, O., Hyde, H. C., Hulse, R. E., and Perozo, E. (2012) Symmetry-Constrained Analysis of Pulsed Double Electron-Electron Resonance (DEER) Spectroscopy Reveals the Dynamic Nature of the KcsA Activation Gate. *J. Am. Chem. Soc. 134*, 16360−16369.
(38) Cady, S. D., Schmidt-Rohr, K., Wang, J., Soto, C. S., DeGrado, W. F., and Hong, M. (2010) Structure of the amantadine binding site of influenza M2 proton channels in lipid bilayers. *Nature 463*, 689−693.
(39) Stouffer, A. L., Acharya, R., Salom, D., Levine, A. S., Di Costanzo, L., Soto, C. S., Tereshko, V., Nanda, V., Stayrook, S., and DeGrado, W. F. (2008) Structural basis for the function and inhibition of an influenza virus proton channel. *Nature 451*, 596−600.
(40) Sharma, M., Yi, M., Dong, H., Qin, H., Peterson, E., Busath, D., Zhou, H., and Cross, T. (2010) Insight into the Mechanism of the Influenza A Proton Channel from a Structure in a Lipid Bilayer. *Science 330*, 509−512.
(41) Luo, W., Cady, S., and Hong, M. (2009) Immobilization of the influenza A M2 transmembrane peptide in virus envelope-mimetic lipid membranes: a solid state NMR investigation. *Biochemistry 48*, 6361−6368.
(42) Klug, C. S., and Feix, J. B. (2008) Methods and applications of site-directed spin labeling EPR spectroscopy, in *Biophysical Tools for Biologists: In Vitro Techniques*, Vol. *1*, pp 617−658, Elsevier Academic Press Inc, London.
(43) Frazier, A. A., Roller, C. R., Havelka, J. J., Hinderliter, A., and Cafiso, D. S. (2003) Membrane-bound orientation and position of the synaptotagmin IC2A domain by site-directed spin labeling. *Biochemistry 42*, 96−105.
(44) Dennison, S., and Phoenix, D. (2011) Effect of Cholesterol on the Membrane Interaction of Modelin-5 Isoforms. *Biochemistry 50*, 10898−10909.
(45) Sood, R., and Kinnunen, P. (2008) Cholesterol, lanosterol, and ergosterol attenuate the membrane association of LL-37(W27F) and temporin L. *Biochim. Biophys. Acta, Biomembr. 1778*, 1460−1466.

DOI: 10.1021/acs.biochem.5b01065
Biochemistry 2015, 54, 7157−7167

(46) Monette, M., Vancalsteren, M., and LaFleur, M. (1993) Effect of cholesterol on the polymorphism of dipalmitoylphosphatidylcholine melittin complexe - an NMR study. *Biochim. Biophys. Acta, Biomembr. 1149*, 319−328.
(47) McMullen, T., Lewis, R., and McElhaney, R. (2004) Cholesterol-phospholipid interactions, the liquid-ordered phase and lipid rafts in model and biological membranes. *Curr. Opin. Colloid Interface Sci. 8*, 459−468.
(48) Altenbach, C., Oh, K., Trabanino, R., Hideg, K., and Hubbell, W. (2001) Estimation of inter-residue distances in spin labeled proteins at physiological temperatures: Experimental strategies and practical limitations. *Biochemistry 40*, 15471−15482.
(49) Jeschke, G., Koch, A., Jonas, U., and Godt, A. (2002) Direct conversion of EPR dipolar time evolution data to distance distributions. *J. Magn. Reson. 155*, 72−82.
(50) Sale, K., Song, L., Liu, Y. S., Perozo, E., and Fajer, P. (2005) Explicit treatment of spin labels in modeling of distance constraints from dipolar EPR and DEER. *J. Am. Chem. Soc. 127*, 9334−9335.
(51) Ghimire, H., McCarrick, R., Budil, D., and Lorigan, G. (2009) Significantly Improved Sensitivity of Q-band PELDOR/DEER Experiments Relative to X-band is Observed in Measuring the Intercoil Distance of a Leucine Zipper Motif Peptide (GCN4-LZ). *Biochemistry 48*, 5782−5784.
(52) Yi, M., Cross, T., and Zhou, H. (2009) Conformational heterogeneity of the M2 proton channel and a structural model for channel activation. *Proc. Natl. Acad. Sci. U. S. A. 106*, 13311−13316.
(53) Fiorin, G., Carnevale, V., and DeGrado, W. (2010) The Flu's Proton Escort. *Science 330*, 456−458.
(54) Howard, K. P., Lear, J. D., and DeGrado, W. F. (2002) Sequence determinants of the energetics of folding of a transmembrane four-helix-bundle protein. *Proc. Natl. Acad. Sci. U. S. A. 99*, 8568−8572.
(55) Hu, F., Luo, W., Cady, S., and Hong, M. (2011) Conformational plasticity of the influenza A M2 transmembrane helix in lipid bilayers under varying pH, drug binding, and membrane thickness. *Biochim. Biophys. Acta, Biomembr. 1808*, 415−423.
(56) Peterson, E., Yi, M., Zhou, H., Sharma, M., Cross, T., and Busath, D. (2010) Acid-Activation, Proton Transport Rate Saturation, and pH-Dependence of Amantadine Block for Influenza a M2 Protein Truncate (22−62). *Biophys. J. 98*, 503A.
(57) Kochendoerfer, G. G., Salom, D., Lear, J. D., Wilk-Orescan, R., Kent, S. B., and DeGrado, W. F. (1999) Total chemical synthesis of the integral membrane protein influenza A virus M2: role of its C-terminal domain in tetramer assembly. *Biochemistry 38*, 11905−11913.
(58) Cady, S., Wang, T., and Hong, M. (2011) Membrane-Dependent Effects of a Cytoplasmic Helix on the Structure and Drug Binding of the Influenza Virus M2 Protein. *J. Am. Chem. Soc. 133*, 11572−11579.
(59) Bowie, J. U. (2001) Stabilizing membrane proteins. *Curr. Opin. Struct. Biol. 11*, 397−402.
(60) Chen, K., Zhou, F., Fryszczyn, B., and Barth, P. (2012) Naturally evolved G protein-coupled receptors adopt metastable conformations. *Proc. Natl. Acad. Sci. U. S. A. 109*, 13284−13289.
(61) Freed, D. M., Horanyi, P. S., Wiener, M. C., and Cafiso, D. S. (2010) Conformational Exchange in a Membrane Transport Protein Is Altered in Protein Crystals. *Biophys. J. 99*, 1604−1610.
(62) Fantini, J., and Barrantes, F. J. (2013) How cholesterol interacts with membrane proteins: an exploration of cholesterol-binding sites including CRAC, CARC, and tilted domains. *Front. Physiol. 4*, 31.
(63) Krause, M., and Regen, S. (2014) The Structural Role of Cholesterol in Cell Membranes: From Condensed Bilayers to Lipid Rafts. *Acc. Chem. Res. 47*, 3512−3521.
(64) Zhao, W., Rog, T., Gurtovenko, A., Vattulainen, I., and Karttunen, M. (2007) Atomic-scale structure and electrostatics of anionic palmitoyloleoylphosphatidylglycerol lipid bilayers with Na+ counterions. *Biophys. J. 92*, 1114−1124.
(65) Epand, R., Thomas, A., Brasseur, R., Vishwanathan, S., Hunter, E., and Epand, R. (2006) Juxtamembrane protein segments that contribute to recruitment of cholesterol into domains. *Biochemistry 45*, 6105−6114.
(66) Epand, R. (2006) Cholesterol and the interaction of proteins with membrane domains. *Prog. Lipid Res. 45*, 279−294.
(67) Barrett, P. J., Song, Y., Van Horn, W. D., Hustedt, E. J., Schafer, J. M., Hadziselimovic, A., Beel, A. J., and Sanders, C. R. (2012) The amyloid precursor protein has a flexible transmembrane domain and binds cholesterol. *Science 336*, 1168−1171.
(68) Thaa, B., Levental, I., Herrmann, A., and Veit, M. (2011) Intrinsic membrane association of the cytoplasmic tail of influenza virus M2 protein and lateral membrane sorting regulated by cholesterol binding and palmitoylation. *Biochem. J. 437*, 389−397.

DOI: 10.1021/acs.biochem.5b01065
Biochemistry 2015, 54, 7157−7167

Supporting Material Available Online: Figures S1-S6

Cholesterol dependent conformational exchange of the C-terminal domain of the influenza A M2 protein

Sangwoo S. Kim,[1] Mary Alice Upshur,[1] Kei Saotome,[1] Indra D. Sahu,[2] Robert M. McCarrick,[2]

Jimmy B. Feix,[3] Gary A. Lorigan,[2] and Kathleen P. Howard[1,]*

1. Department of Chemistry and Biochemistry, Swarthmore College, Swarthmore, PA 19081

2. Department of Chemistry and Biochemistry, Miami University, Oxford, OH 45056

3. Department of Biophysics, National Biomedical EPR Center, Medical College of Wisconsin, Milwaukee, WI 53226

Figure S1. Representative saturation recovery traces for M2TMC-I42C (top) and M2TMC-I51C (bottom) in POPC:POPG (4:1) under 100% air and 40% air, respectively. The red lines are the double exponential fits to the data (black lines). Shown on the right are the corresponding residuals (magnified 5x) for single and double-exponential fits indicating the relaxation is bi-exponential and indicative of conformational exchange between two components.

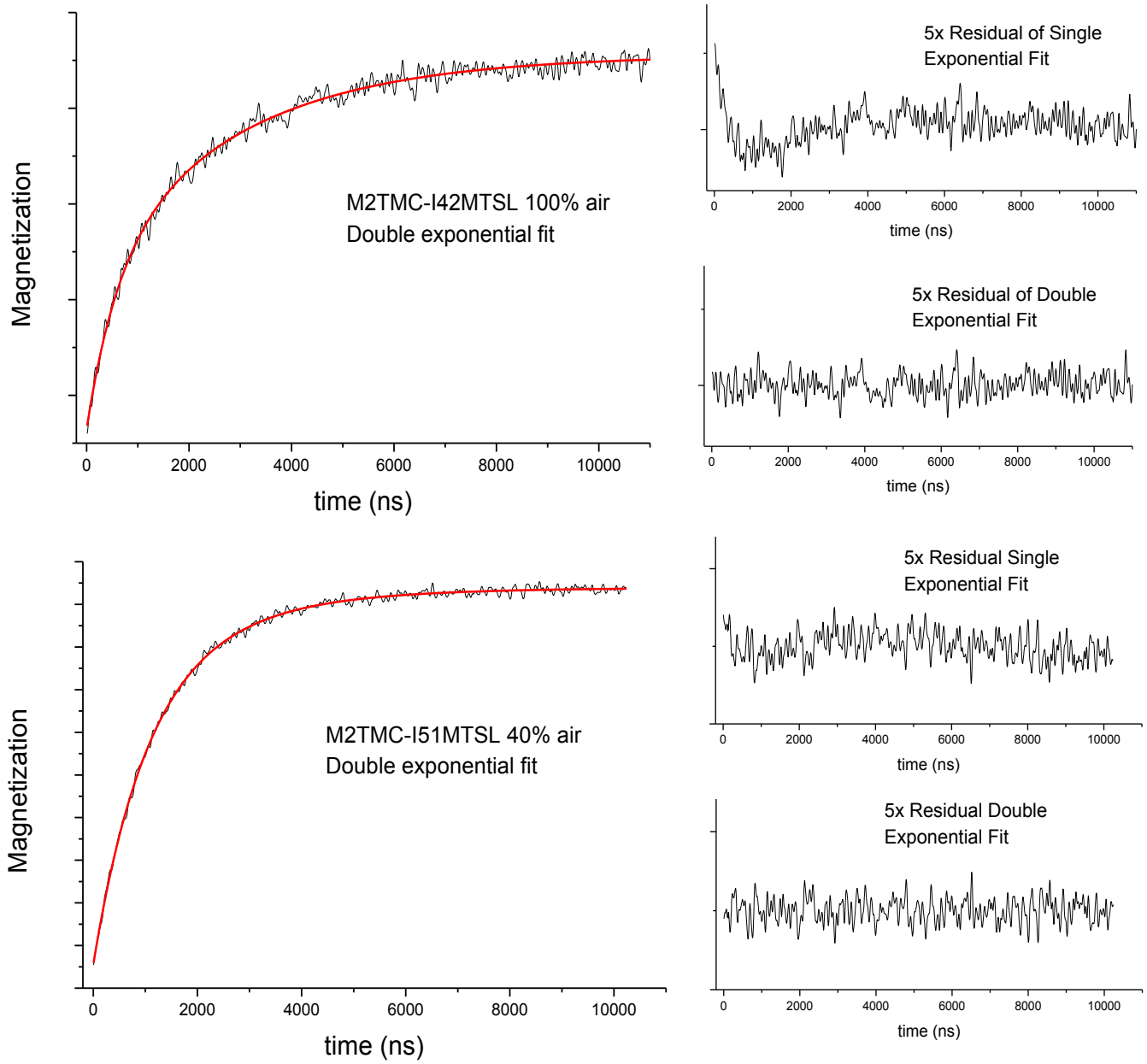

Figure S2. CW-EPR spectra of five mutants of M2TMC in POPC:POPG (4:1) bilayers in the absence (left) and presence of cholesterol (right). Samples contained either four spin-labeled monomers per tetramer (fully-labeled, red), or one spin-labeled monomer per tetramer (dilute-labeled, black). Spectra were normalized for number of spins and central peak intensities were used to calculate the Ω values shown in Figure 6C.

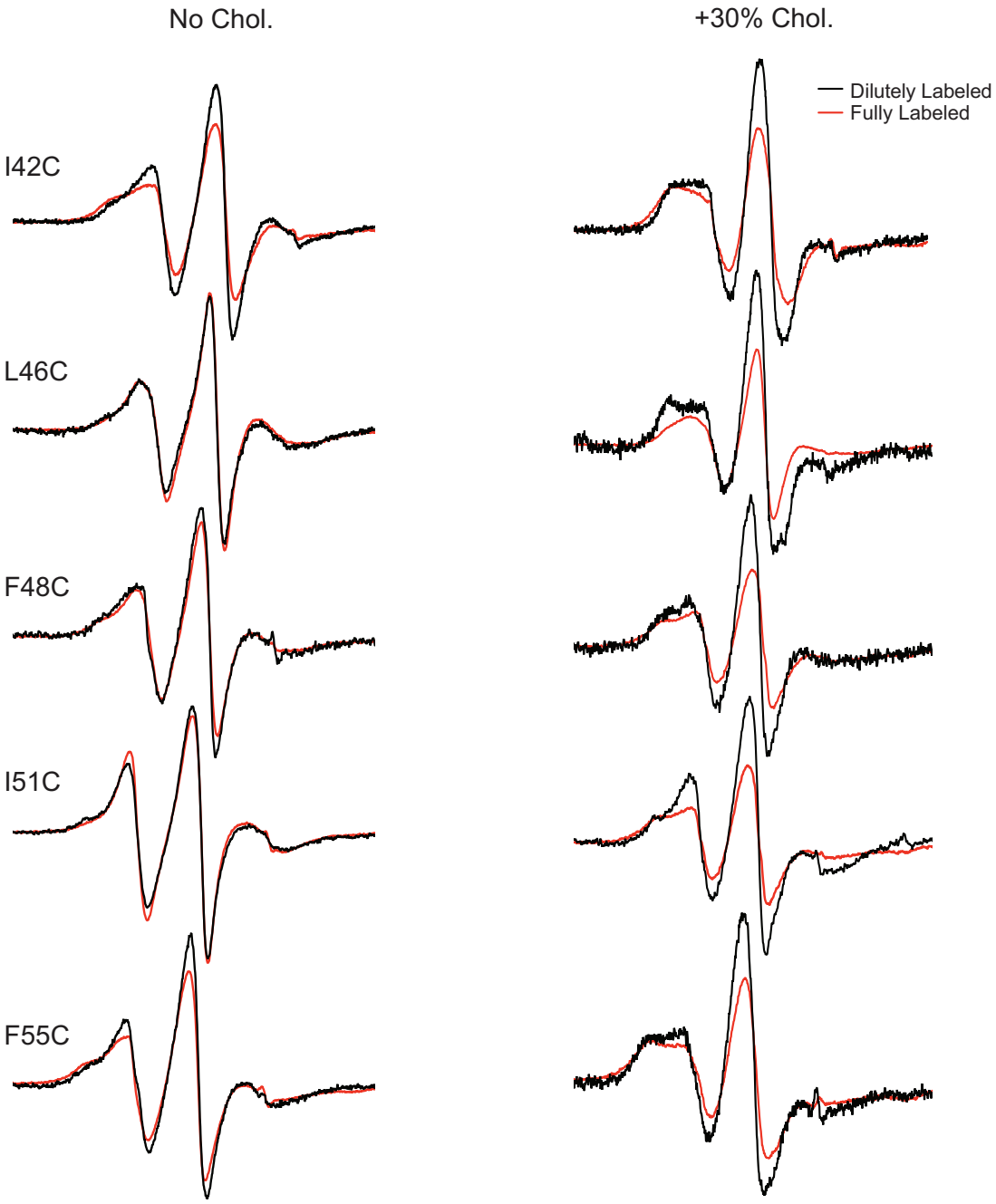

Figure S3. Hypothetical DEER distance distributions for a spin-labeled homotetrameric protein. Top Panel: When only one conformation is present, two distances are expected; distance "a" is the proximal distance between two subunits and distance "b" diagonal distance between two subunits. Bottom Panel: When a sample includes a mixture of two unique conformations, four peaks are expected in the DEER distribution. For a symmetric homotetramer, b/a and c/d should be approximately 1.414. Adapted from Dalmas et al. 2012.

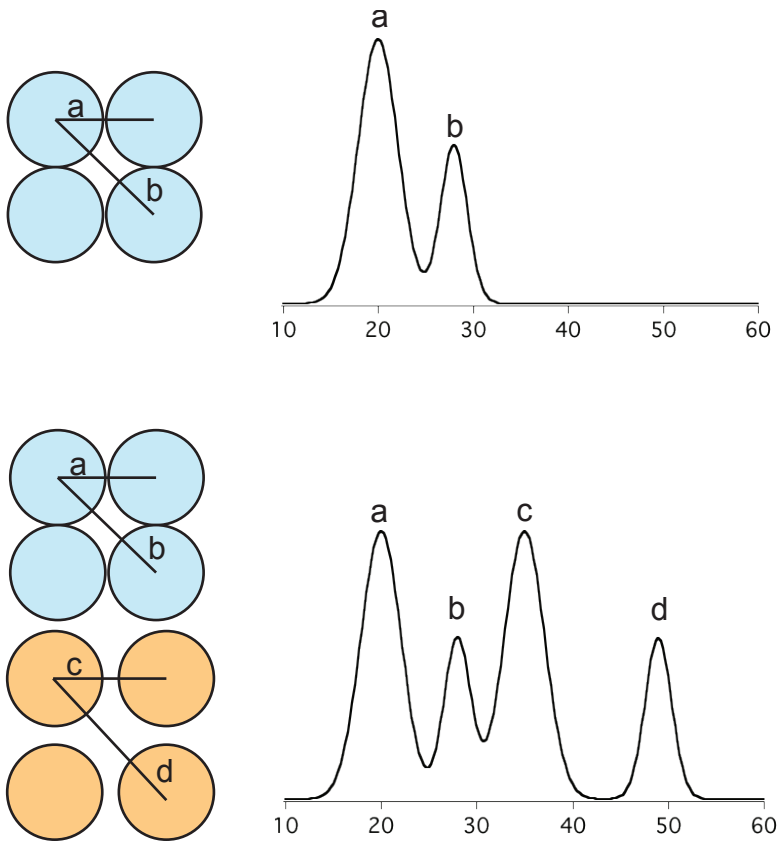

Figure S4. Tikhonov L-curve for M2TMC-I51C (left) and M2TMC-F55C (right) for DEER data shown in Figure 7. The highlighted red data points represent regularization parameters used to obtain distance distributions (λ=40 for M2TMC-I51C and λ=25 for M2TMC-F55C).

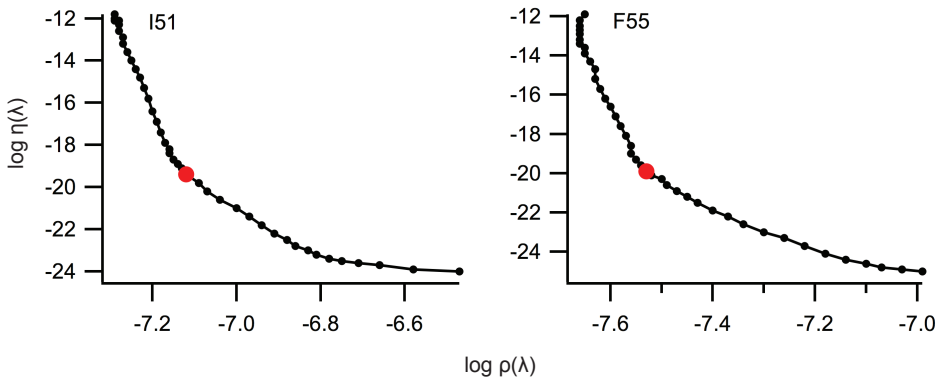

Figure S5. A. Tikhonov Regularization and distance distributions of M2TMC-I51C in bicelles (λ=16, top) and Lipodisqs (λ=631, middle), and M2TMC-F55C in Lipodisq (λ=251, bottom). Experimental DEER data in micelles is shown in Figure 7. B. Overlay of distance distributions of M2TMC-I51C in micelles (black), bicelles (blue), and Lipodisq (red). C. Overlay of distance distributions of M2TMC-F55C in micelles (black) and Lipodisq (red).

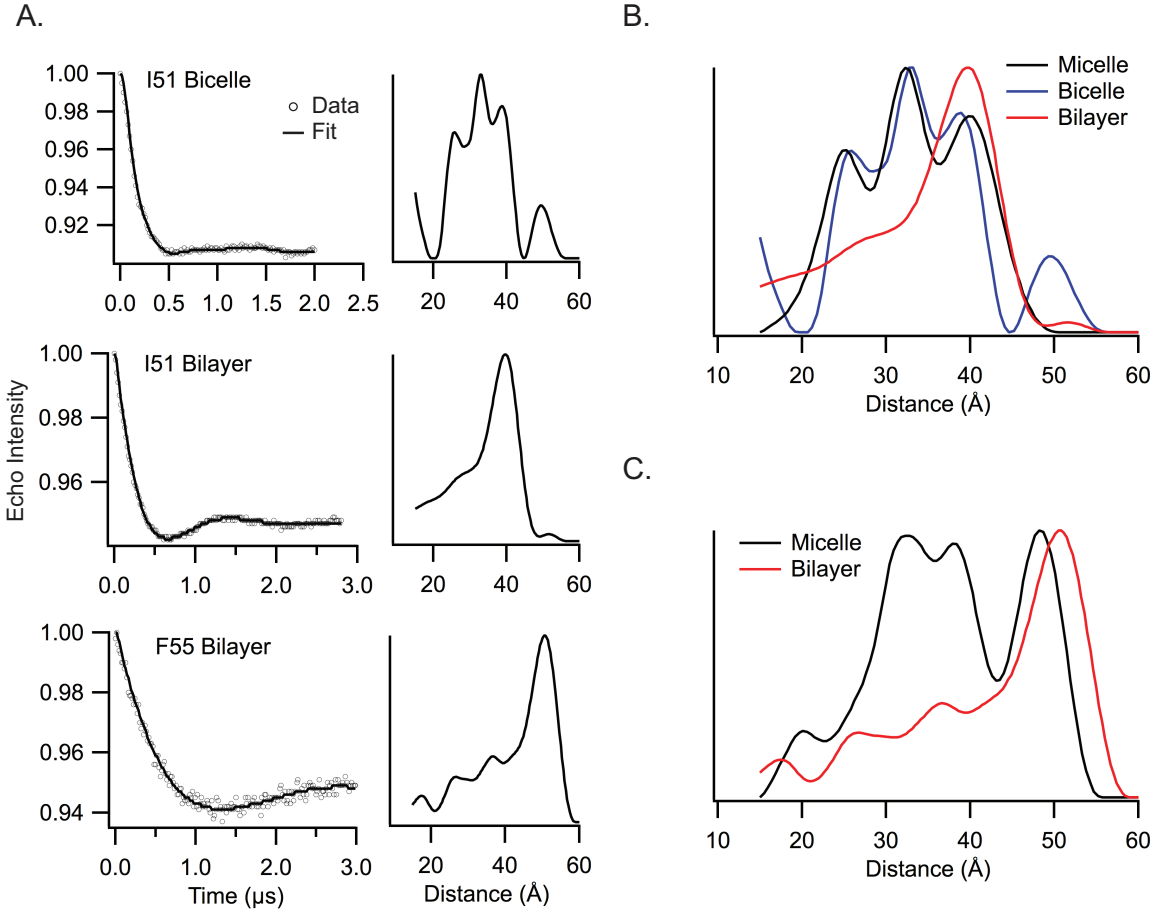

Figure S6. Comparison of ssNMR model (PDB 2L0J) with experimental DEER data. A. Side view and B. top down view of ssNMR model. Proximal and diagonal distances for I51 and F55 are listed as (proximal, diagonal) in Å. Distances were measured between $H_{C,\gamma}$ of corresponding sites from the published ssNMR model (PDB 2L0J). The diagonal distances for both I51 and F55, 24 and 19 Å respectively, are in close agreement with our DEER data shown in Figure 7. The proximal distances for both I51 and F55, 17 and 15 Å respectively, are below the reliable detection limit of DEER (shown by gray box). C. Simulations of DEER distances distributions using distances between I51 and F55 within the tetramer as measured from ssNMR model 2L0J.